Modeling the effects of topography and wind on atmospheric dispersion of CO_2 surface leakage at geologic carbon sequestration sites

Fotini K. Chow[a],*, Patrick W. Granvold[a], and Curtis M. Oldenburg[b]

[a]*Department of Civil and Environmental Engineering, University of California, Berkeley, CA 94720-1710, USA*
[b]*Earth Sciences Division, Lawrence Berkeley National Laboratory, 1 Cyclotron Rd., MS 90-1116, Berkeley, CA 94720, USA*

Abstract

Understanding the potential impacts of unexpected surface releases of CO_2 is an essential part of risk assessment for geologic carbon sequestration sites. We have extended a mesoscale atmospheric model to model dense gas dispersion of CO_2 leakage. The hazard from CO_2 leakage is greatest in regions with topographic depressions where the dense gas can pool. Simulation of dispersion in idealized topographies shows that CO_2 can persist even under high winds. Simulation of a variety of topographies, winds, and release conditions allows the generation of a catalog of simulation results that can be queried to estimate potential impacts at actual geologic carbon sequestration sites.

1. Introduction

An essential component of risk assessment at geologic carbon sequestration sites is the estimation of the impact and likelihood of unexpected surface releases of CO_2. Carbon dioxide gas can potentially migrate through faults, fractures, or abandoned wells that may provide pathways for leakage to the ground surface. Though such leakage is typically slow and in small amounts if it can occur at all, negatively buoyant CO_2 may accumulate at the ground surface under calm conditions, posing health risks to humans and animals in the vicinity. Prior studies have suggested that wind-driven dispersion would be effective at dispersing leaking CO_2 [1], but the model was unable to represent dense gas effects above the ground surface that could inhibit mixing. Because atmospheric dispersion of CO_2 is driven by gravity (gas-density contrast) and wind, the danger from CO_2 is greatest in regions with topographic depressions where the dense gas can pool, or under stably-stratified background atmospheric conditions which further inhibit mixing and dilution of the gas. In this work, we have extended a mesoscale atmospheric model to predict dispersion of releases of dense CO_2 gas. Simulation of dispersion in idealized topographies illustrates the

----

* Corresponding author. Tel.: +1-510-643-4405; fax: +1-510-642-7483.
E-mail address: chow@ce.berkeley.edu.

ability of common topographic depressions to trap accumulated CO_2 for extended periods and at concentrations that exceed limits allowable for continuous or instantaneous exposure; accumulated CO_2 can persist for shorter periods even under high ambient winds. A variety of simulations of different release strengths and background atmospheric conditions allows the generation of a catalog of results that can be queried to identify hazardous scenarios, illustrating the utility of the model for risk assessment and certification of carbon sequestration sites. In future work, the model will be applied to proposed pilot geologic sequestration target formations (e.g., the Mt. Simon Formation, IL, and the San Joaquin Valley, CA) to evaluate CO_2 release risks at those sites should CO_2 leakage occur.

2. Numerical formulation

The simulations are performed using a mesoscale atmospheric model, the Advanced Regional Prediction System (ARPS). ARPS is a numerical weather prediction code that allows specification of complex terrain, land-surface fluxes, heterogeneous land cover, time-dependent weather forcing, etc. Here, ARPS has been modified to simulate dense gas dispersion appropriate for CO_2 leakage from geologic carbon sequestration sites. ARPS was developed at the Center for Analysis and Prediction of Storms at the University of Oklahoma, and can be run as a large-eddy simulation (LES) code that solves the three-dimensional, compressible, non-hydrostatic, filtered Navier-Stokes equations. Fourth-order spatial differencing is used for the advection terms. Temporal discretization is performed using a mode-splitting technique to accommodate high-frequency acoustic waves. The large time steps (Δt) use the leapfrog method; first-order forward-backward explicit time stepping is used for the small time steps ($\Delta \tau$), except for terms responsible for vertical acoustic propagation, which are treated semi-implicitly. ARPS is described in detail by Xue et al. [2,3].

ARPS was previously modified to include a scalar-advection diffusion equation (see Michioka and Chow 2008). Here, the formulation is modified to allow for dense gas transport, and takes the form

$$\frac{\partial \rho X_c}{\partial t} + u\frac{\partial \rho X_c}{\partial x} + v\frac{\partial \rho X_c}{\partial y} + w\frac{\partial \rho X_c}{\partial z} = \frac{\partial}{\partial x}\left(\kappa_T \frac{\partial \rho X_c}{\partial x}\right) + \frac{\partial}{\partial y}\left(\kappa_T \frac{\partial \rho X_c}{\partial y}\right) + \frac{\partial}{\partial z}\left(\kappa_T \frac{\partial \rho X_c}{\partial z}\right) \quad (1)$$

where X_c is the mass fraction of the gas in a particular cell, u, v, and w are the velocity components in the x, y, and z directions, respectively, κ_T is the turbulent eddy diffusivity, and ρ is the total density in kg/m^3. Note that the entire quantity ρX_c is solved for at each time step (i.e., the two quantities are not calculated separately). Active scalar (i.e., dense gas) transport required modifying two areas of the model: (1) calculation of density, and (2) calculation of buoyant forcing in the w-equation. This allows incorporation of the total density (due to air and the dense gas) into the buoyancy forcing, which appears in the vertical momentum equation. The density field thus couples the equation describing transport and dispersion of the dense gas with the momentum equations, causing the model to feel the effects of density-driven flow. Note that the ARPS system of governing equations does not allow for large mass fluxes across a boundary, hence the current formulation can accommodate instantaneous releases only.

3. Passive vs. dense gas dispersion

The behavior of dense gases such as CO_2 can be quite different than for passive tracers (with neutral buoyancy) due to density effects [4]. For example, a plume of CO_2 will spread laterally over flat terrain even in the absence of wind because it is denser than the surrounding air. A concentrated CO_2 plume will generally hug the ground and cross terrain contours to reach the lowest elevation. Driven by density effects, a CO_2 plume will spread more quickly than a neutrally-buoyant gas which spreads only through diffusion, giving the counter-intuitive result that ground-level concentrations can drop more quickly for a dense gas than for a passive gas tracer under calm conditions. The problem and risk for prolonged exposure to CO_2 at high concentrations, however, lies in the fact that topographical depressions or basins provide preferential sites for accumulation and immobilization. The presence of negatively buoyant gas in sufficient amounts can prevent the scouring of the gas from a basin by ambient winds.
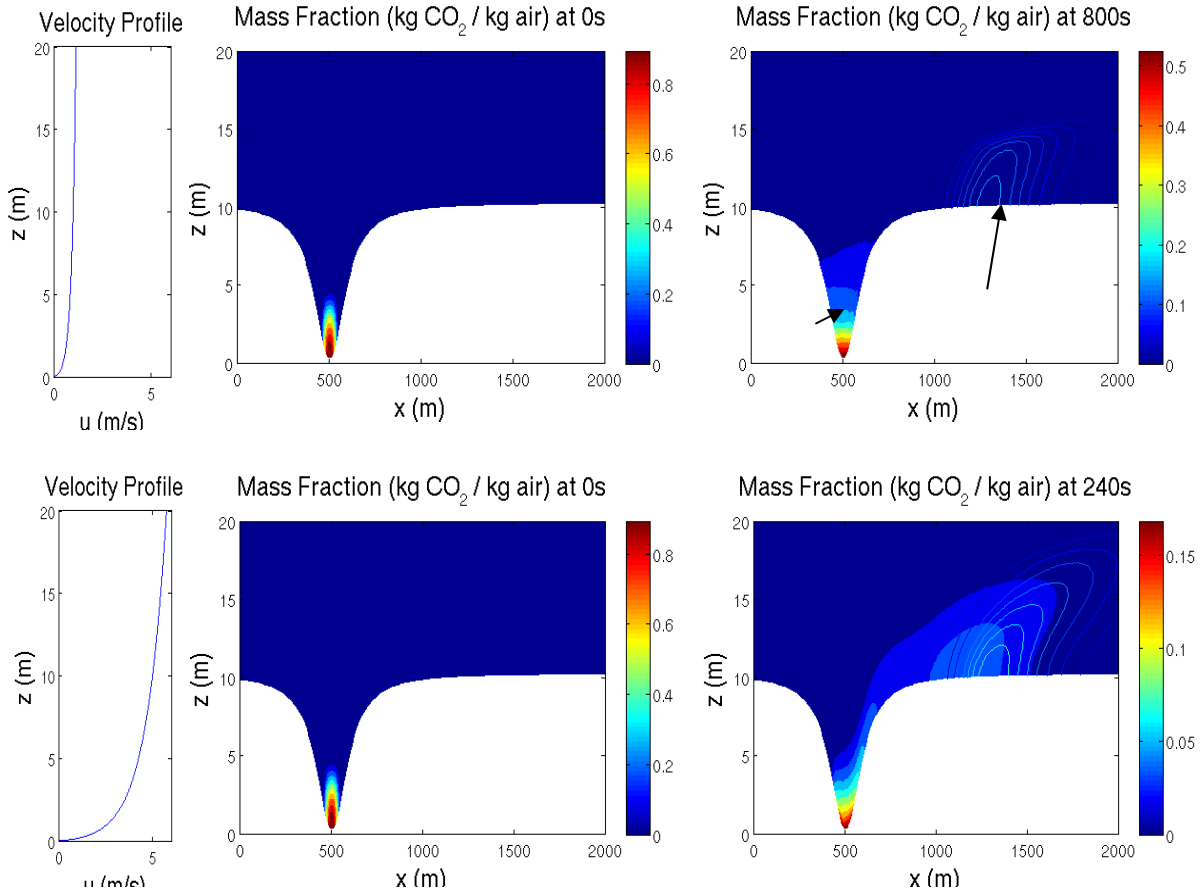
2

Figure 1. Scouring from a 2D trench. Solid filled contours show mass fraction of CO_2, solid lines show passive tracer. Profiles on left indicate driving wind at left edge of domain.

The impact of topography and ambient conditions on scalar dispersion can be illustrated through examination of a two-dimensional idealized basin described by mirror sigmoid functions. Simulations were performed on a computational domain of 200 x 60 grid cells, with $\Delta x = 5$ m and a stretched grid in the vertical with a minimum resolution of $\Delta z = 0.25$ m and an average resolution of 2 m. The top and bottom boundaries are rigid, and there is a Rayleigh damping layer beginning at $z = 80$ m. An instantaneously released mass of CO_2 is initialized at the bottom of a depression. A logarithmic wind profile is initialized across the domain and held constant as an inflow condition on the left, as shown in Figure 1. Figure 1 shows the difference between scouring of a passive scalar (no density effects, solid lines) and CO_2 (dense gas, color contours). The passive scalar is quickly transported out of the basin, while the CO_2 plume lingers in the basin even under strong winds (~5 m/s).

4. CO_2 dispersion over idealized complex terrain

To investigate the behavior of CO_2 dispersion and accumulation under various conditions, a catalog of simulations was created for different topographies, release scenarios, and meteorological conditions. Together, these simulations comprise an example database a user could query to quickly identify potential hazards at a proposed CO_2 sequestration site for risk assessment purposes. The choice of parameters is described first, followed by discussion of key findings from the simulations.

4.1. Terrain and model setup

Four types of terrain were used in the simulation scenarios: (A) completely flat ground, (B) flat ground interrupted by a long trench of depth 10 m, (C) flat ground interrupted by a step change in elevation (shelf) of 10 m (a half-trench), and (D) a set of rolling hills of maximum amplitude 50 m (see Figure 2). The domain size is (203, 143, 43) grid points in the x, y, and z directions, respectively, for all cases except the rolling terrain where it is (163, 203, 43). The simulations all use the same grid spacing ($\Delta x = \Delta y = 5$ m, $\Delta z_{avg} = 2.5$ m, $\Delta z_{min} = 0.25$ m near the ground, stretched above) and time steps ($\Delta t = 0.02$ s, $\Delta \tau = 0.002$ s). Lateral boundary conditions are zero-gradient. Top and bottom boundaries are rigid walls, with a log-law condition specified at the bottom boundary to account for surface drag (as is typical in all mesoscale prediction models). A Rayleigh damping layer is used at the top of the domain above 80 m. All simulations use a 1.5 order turbulent kinetic energy formulation for the large-eddy simulation turbulence closure.
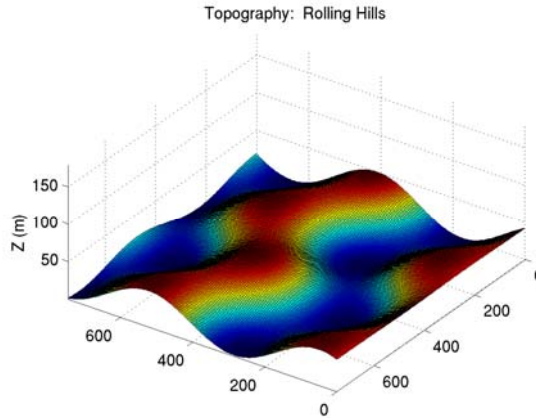

Figure 2. Rolling terrain used for catalog of ideal simulations.

4.2. Ambient wind speed

The dispersion of CO_2 is highly dependent on ambient winds. In weak winds, density (buoyancy) effects dominate the dispersion process; in high winds, the gas begins to act more as a passive pollutant, with the ambient wind overwhelming density effects. Because local hazard is highest when CO_2 is allowed to pool or concentrate in topographical features, wind speeds were primarily chosen from calm or near-calm conditions, with fewer scenarios using high wind speeds. Wind speeds were chosen from the following set: 0 m/s (calm conditions), 0.5 m/s, 1 m/s, 2 m/s, and 4 m/s. Winds were initialized uniformly over the domain. Shear develops at the ground after the simulation is started due to drag at the surface (corresponding to an effective roughness height of 0.1 m). A range of wind directions can be selected but winds from the west were applied in the cases shown here.

4.2.1. Atmospheric stability

The stability of the atmosphere can affect the vertical and horizontal dispersion of a dense gas. In the presence of a highly stably stratified atmosphere (such as is common during the night), vertical dispersion is inhibited, horizontal dispersion can be enhanced, and kinetic energy is required to break down the stratification to allow vertical mixing. The stability of the atmosphere is represented by the square of the Brunt-Vaisala frequency, N:

$$N^2 = g / \theta \ (\partial \theta / \partial z) \tag{2}$$

4

where g is the gravitational acceleration, θ is the potential temperature of the air (here taken to be at the surface), and $\partial\theta/\partial z$ is the vertical potential temperature gradient. For neutral conditions, N^2 is zero, and no density gradient exists to inhibit mixing. For stably stratified conditions, N^2 is positive. A value of $N^2 = 0.000327$ s^{-2} is selected for comparisons; this yields weakly stable conditions with a temperature gradient of approximately 0.01 K/m.

4.2.2. Release strength

Releases are considered to be instantaneous, with a magnitude of either 1,000 kg (1 tonne) or 10,000 kg (10 tonnes) of CO_2 at the surface. A uniform hemispherical instantaneous release is specified, with a radius of 15 m in x and y and 6 m in z for the 1,000 kg release, or 30 m in x and y and 14 m in z for the 10,000 kg release.

4.2.3. Plume statistics

For each case scenario, a number of parameters are extracted for analysis of plume extent and dilution time. Three concentration threshold levels are chosen which correspond to a Short-Term Exposure Level (STEL) for 15 minutes. The thresholds are based on mass fractions (i.e. kg CO_2/kg air) of 0.01, 0.03, and 0.1, which correspond to concentrations of 10,000 ppm (1%), 30,000 ppm (3%), and 100,000 ppm (10%). Severe headaches, diffuse sweating, and labored breathing begin at 30,000 ppm. The OSHA, NIOSH, and ACGIH occupational exposure standards are 0.5% CO_2 for a 40-hour work week average and 3% for a 15-minute exposure. The maximum instantaneous limit is 4%. All three exposure standards must be satisfied [5]. In addition to plume extent, local exposure times (in seconds) are provided for each of the chosen thresholds. Thus, if the overall exposure time is greater than 900 s (15 min) for the 0.03 mass fraction threshold, the STEL will have been exceeded.

A series of three figures showing ground level concentration at 300 s, 600 s, and 900 s is provided for each simulation. A second series of three figures shows the amount of time spent above the three threshold concentrations as a function of x,y location, indicating which portion of the domain is at risk for exceeding the STEL. Two examples are given in Figure 3 and Figure 4 for the rolling hills: case D1 with no ambient winds, and case D1 with a 1 m/s westerly wind. Both are initialized with a 10 tonne release of CO_2. The source location is marked with an 'x'. With no winds, the CO_2 flows downhill and collects in the valley. With a 1 m/s wind, the primary direction of plume spreading is still down-gradient (perpendicular to the mean wind direction), with significant accumulation in the valley. A portion of the plume even travels upwind of the source location. A large area in the valley exceeds the 0.01 threshold, and a smaller area exceeds the 0.03 concentration threshold for more than 15 minutes. Note that the threshold contours and statistics are calculated based on data at 60 s intervals.

4.2.4. Key findings

A set of 22 simulations was performed to investigate the parameter spaces described above, including topography type, wind speed, stability, and release strength. A brief summary of findings is given here. With zero winds and flat terrain, the CO_2 plume spreads symmetrically from the initial source location as expected. Terrain and non-zero winds change the plume shape and orientation. Increased wind speed causes the initial CO_2 plume to be lifted off the ground due to the wind shear, leading to lower ground level concentrations and faster dilution (see example in Figure 5 for 1 m/s winds over flat terrain).

Topographic depressions inhibit the movement of the CO_2 plume under weak winds. At wind speeds of greater than 2 m/s, the plume is quickly swept out of the domain and diluted, even for rolling hills of amplitude 50 m. The
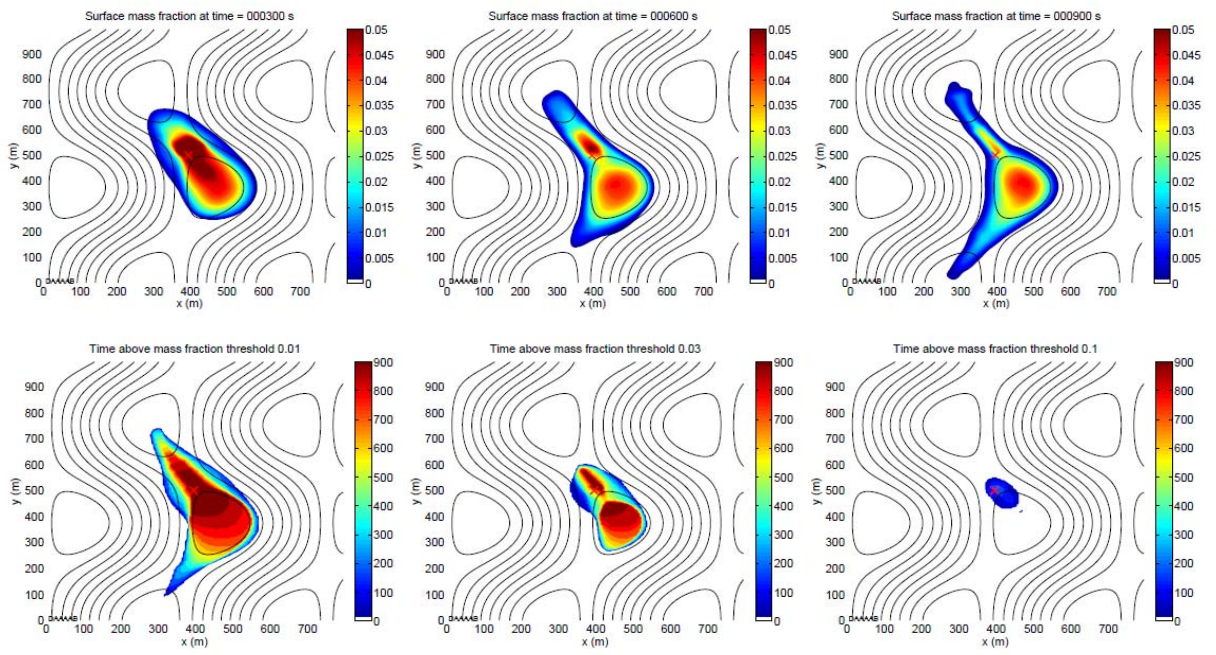
Figure 3. Case D1. Rolling hills with no winds, 10 000 kg release (marked by 'x'). Top panel shows surface CO_2 mass fraction contours. Bottom panels show exposure time above each threshold level (in seconds). Black lines show terrain contours.
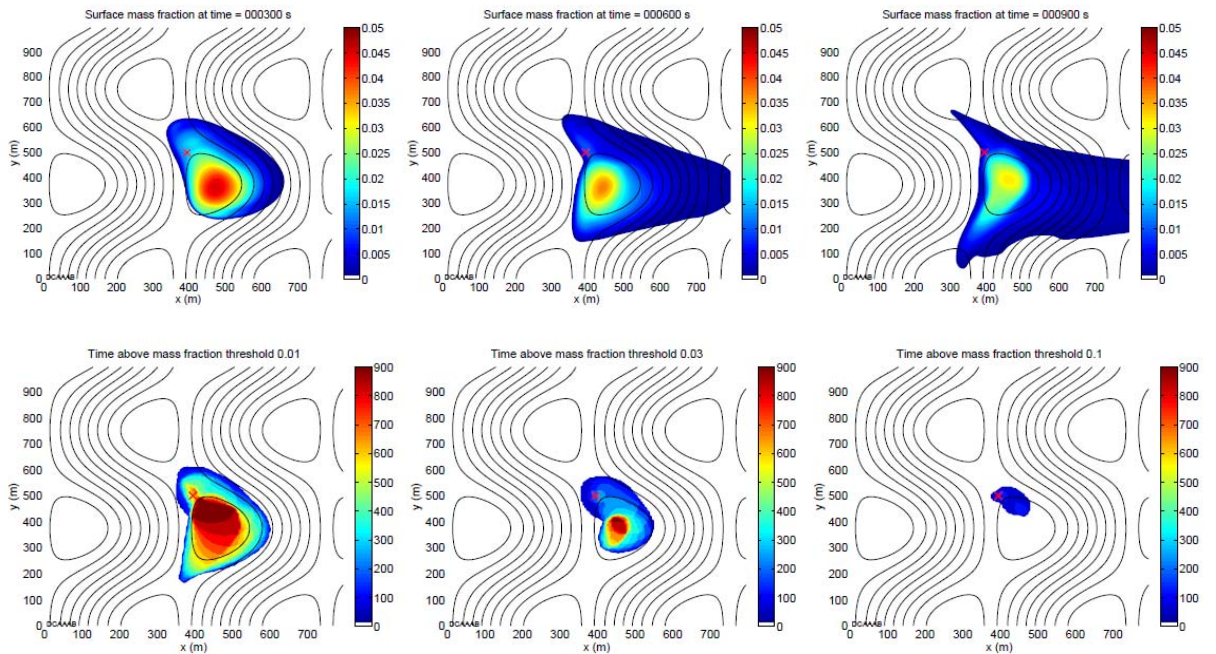

Figure 4. Case D2. As in Figure 3 but for 1 m/s background winds.

CO$_2$ plume disperses "downhill" due to gravity and can thus move perpendicular to the mean wind direction (as in the rolling hills cases shown above in Figure 3). As the plume attempts to move out of the valley, a gravity current return flow is generated with flow that opposes the mean wind direction, as shown in Figure 6 below. Topography can also inhibit the movement of the CO$_2$ plume by blocking the spread in a certain direction, and can trap a portion of the plume (in the trench, half-trench, and rolling hills cases). The plume is partially trapped even with a trench or half-trench height of only 10 m (see Figure 7, below).

The 0.01 concentration STEL is exceeded in all cases with zero winds. For cases with non-zero winds, only a few cases, all at 0.5 or 1.0 m/s, exceeded the 0.01 threshold. The 0.03 concentration STEL is exceeded in even fewer cases, one for rolling hills with a 1 m/s wind, while the other cases are all calm (zero winds). Larger release strengths (10 000 kg) lead to larger plume extent and exposure times.

Atmospheric stability leads to an increase in horizontal plume extent for the cases with 1 m/s winds. The time to dilution increases slightly with stability. For the hilly terrain, stable stratification with a 1 m/s wind showed the largest difference compared to the neutral stratification. With a stable atmosphere, the plume is trapped in the topographic depression and this leads to the STEL being exceeded with 1 m/s winds that is not observed under neutral conditions. With no wind, the differences due to atmospheric stability are negligible. Overall, atmospheric stability does not have as large an effect as the parameter values explored for wind speed, terrain type, or source strength.
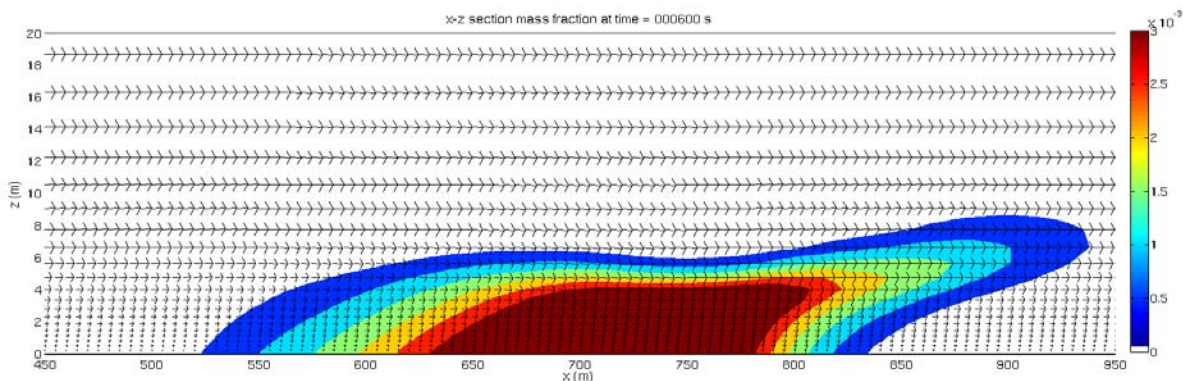

Figure 5. Vertical cross section (*x-z* plane) from flat terrain case with 1 m/s winds, 1,000 kg release, at *t* = 600 s showing contours of mass fraction and wind vectors. The plume is advected in the direction the mean westerly wind and is lifted above the ground.
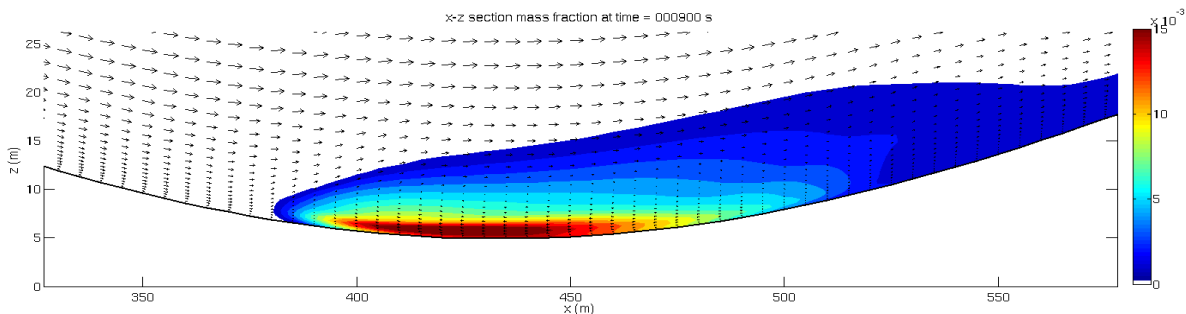

Figure 6. Vertical cross section (*x-z* plane) from rolling hills case with 1 m/s winds, 10,000 kg release, at *t* = 900 s showing contours of mass fraction and wind vectors. There is reverse flow near the ground on the right side of the valley which opposes the mean westerly wind aloft.
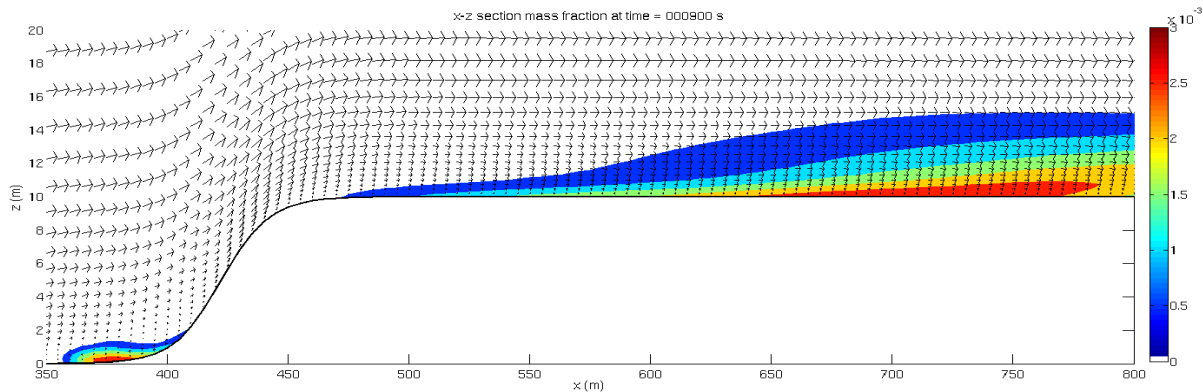
Figure 7. Vertical cross section (x-z plane) from half-trench case with 1 m/s winds, 1,000 kg release, at $t = 900$ s showing contours of mass fraction and wind vectors. There is reverse flow near the ground to the left of the ridge which opposes the mean westerly wind aloft leading to part of the plume being trapped by the topography.

5. Conclusions and future work

We have modified the mesoscale atmospheric weather prediction code ARPS to study dense gas dispersion of CO_2 releases under various conditions. A catalog of idealized simulation results was created to demonstrate features of dense gas dispersion and to create a tool to allow stakeholders to carry out risk assessment for a particular CO_2 storage site by querying a database. The effects of topography, wind speed, atmospheric stability, and release strength on plume dispersion were explored. It was found that even topographic depressions of 10-50 m in depth can lead to accumulation of CO_2 at hazardous exposure levels. Future work will investigate the dispersion of CO_2 leakage at actual geologic carbon sequestration pilot sites under a variety of atmospheric conditions. It is likely that real terrain will exhibit elevation changes and topographic variations that are least on the order of 10 m at some sites, indicating the need for further investigation for risk assessment purposes.

6. Acknowledgements

References

1. Oldenburg, CM, and AJA Unger, Coupled vadose zone and atmospheric surface-layer transport of CO_2 from geologic carbon sequestration sites, *Vadose Zone Journal*, *3*, 848–857, 2004.
2. Britter, RE, Atmospheric Dispersion of Dense Gases, *Annual Reviews of Fluid Mechanics*, *21*, 317-344, 1989.
3. Xue, M, KK Droegemeier and V Wong: The Advanced Regional Prediction System (ARPS): A multi-scale nonhydrostatic atmospheric simulation and prediction model. Part I: Model dynamics and verification., *Meteorol. and Atmos. Phys.*, *75*, 161-193, 2000.
4 Xue, M, KK Droegemeier, V Wong, A Shapiro, K.Brewster, F Carr, D Weber, Y Liu and D Wang: The Advanced Regional Prediction System (ARPS): A multi-scale nonhydrostatic atmospheric simulation and prediction tool. Part II: Model physics and applications, *Meteorol. and Atmos. Phys.*, *76*, 143-165, 2001.
5. Benson, SM, R Hepple, J Apps, C-F Tsang, and MJ Lippmann. Lessons learned from natural and industrial analogues for storage of carbon dioxide in deep geologic formations, Lawrence Berkeley National Laboratory Report *LBNL-51170*, 2002.

8